Rock Mech Rock Eng (2017) 50:3073–3084
DOI 10.1007/s00603-017-1267-2

ORIGINAL PAPER

A Comminution Model for Secondary Fragmentation Assessment for Block Caving

René Gómez[1,4] · Raúl L. Castro[2,3,4] · Aldo Casali[3] · Sergio Palma[2,3,4] · Asieh Hekmat[1,2,3]

Received: 12 September 2016 / Accepted: 20 June 2017 / Published online: 3 July 2017

Abstract Predicting the rock fragmentation obtained in drawpoints or secondary fragmentation is crucial in Block caving application since many engineering decisions are based on this key variable. These can include drawpoints size and spacing, equipment selection; draw control procedures, production rates, dilution entry and operational blasting requirements. Secondary fragmentation depends on several variables including structures, rock mass strength, the vertical pressure acting on the column, the rate of draw, and the height of the ore column. In order to study these variables, 18 experiments on gravity flow under confinement were run to quantify the fragmentation occurring in a draw column. Based on these experiments, a mathematical model was developed the basis of which considers a modified comminution model fitted using the experimental data. Finally, the fitted model was scaled up to represent what is expected to occur in practice compared to field data with an estimated accuracy of around 1.5% of size distributions. An approximation of the secondary fragmentation expected as a function of draw height and vertical pressure, for example for 400 m of ore column (mean vertical pressure of 4.2 MPa), the mean size, d_{50}, could decrease from 0.82 to 0.47 m and the large size, d_{80}, from 1.08 to 0.62 m.

Keywords Block caving · Secondary breakage · Comminution · Rock · Gravity flow · Formula · Confined flow experiments · Model tests and vertical pressure

1 Introduction and Literature Review

Due to lower commodity cost, lower grades, and deeper deposits, the caving mining industry has encouraged the demand for increased productivity and reducing costs (Flores 2014). In Block caving, feasible production schedule/budgeting is highly influenced by drawpoint reliability, which is largely controlled by fragmentation. The process of fragmentation in caving mines has been classified as: in situ, primary and secondary fragmentation (Laubscher 1994). In situ fragmentation is related to the size of the blocks defined by the joints in the rock mass, prior to mining activities. Primary fragmentation is related to the size of the blocks as a result of induced stresses acting on the cave back. Secondary fragmentation, which occurs after primary fragmentation, is related to the movement of the fragmented rocks toward the drawpoints (Brown 2004). The degree of secondary fragmentation depends on several variables including primary fragmentation, the stress acting within the caved mass, the rock mass strength, the rate of draw, and the height of the ore column (Laubscher 1994; Eadie 2003; Brown 2004).

It has been observed at the mines that fragmentation decreases as more draw is conducted at drawpoints. Primary fragmentation increases over time due to higher cave back stresses as the column height increases, while secondary fragmentation mainly contributes increasing the

✉ René Gómez
regomez@udec.cl

[1] Department of Metallurgy, University of Concepción, Concepción, Chile

[2] Advanced Mining Technology Center, University of Chile, Santiago, Chile

[3] Department of Mining Engineering, University of Chile, Santiago, Chile

[4] Block Caving Laboratory, University of Chile, Santiago, Chile

distance that fragments have to descend through the caved column, also increasing its residence time.

In terms of modeling, some authors have used numerical methods to describe the secondary fragmentation (Chitombo 2010; Esterhuizen 2005; Pierce 2009). These methods can be classified as empirical methods: gravity flow and comminution mechanisms.

The most widely used tools for assessing primary and secondary fragmentations in Block Caving operations is the Block Cave Fragmentation (BCF) software (Esterhuizen 2005). BCF was specifically developed to generate rock size distribution using input data as: primary fragmentation outcomes, aspect ratio of blocks, block strength, cave pressure (overload), stress induced by arching, height of draw, and additional fine material. When a block is under breakage in BCF, it is split into two new equal blocks with lower aspect ratios than the original, and these new blocks can be split again a fixed number of times. BCF also considers the rounding of block and fine material generation. Although it is being used around the globe, there are several shortcomings of BCF in estimating secondary fragmentation as it is based on rule of thumb to estimate how rocks fragments during flow. Furthermore, the model does not consider the rock's fracture mechanics, or the residence time of blocks within draw columns (e.g., two blocks as starting at the same height of draw could go down drawpoint at difference times). Using actual data from Premier and Codelco caves in Chile, Ngidi and Pretorius concluded that BCF predictions are generally conservative (Ngidi and Pretorius 2010).

In terms of gravity flow, secondary fragmentation has been modeled considering shearing and compression mechanisms within caved mass (Pierce 2009). Pierce (2009) developed Rebop, in which he introduced a complete background based on the empirical approach to define the breakage of the compressed angular materials under low pressures suggested by Hardin (1985) and the role of shearing (Bridgwater et al. 2003). Pierce has indicated that in the movement zone there are very low isotropic stresses and most of the fragmentation is expected to occur due to shear stress at the IMZ boundary. And in the stagnant zone where high anisotropic stresses are predominant, so splitting by compression is prevalent. Here, two relevant parameters are not taken into account such as the time material resides in the draw zone and the block's shape (aspect ratio). Initial simulation compared with mine data showed an overestimation of the degree of fragmentation (Pierce 2009). Better results were obtained considering an hybrid methodology described by Pierce et al. (2010).

Another approach to model secondary fragmentation has been through the application of comminution models (the Matrix Model; Merino 1986). It is a method that could be used to study the process of comminution and has been successfully applied to comminution in grinding machines (National Materials Advisory Broad 1981). This methodology is based in a mass balance of fragments, considering concept as rate of breakage, size distribution, residence time distribution, and a mathematical description of the fragmentation processes. Useful to be experimentally developed, then, it is suitable for the study of any breakage process including secondary fragmentation in caving. Even though it has been applied to caving environments, there is no experimental evidence of the efficiency of this matrix model.

While being simple to apply, empirical models lack a theoretical or experimental background to explain the gravity flow variables in the fragmentation process of Block Caving. There is evidence that compression and shear have influence on fragmentation (Pierce et al. 2010). In this article, a comminution model as well as experimental results about secondary fragmentation during flow is presented. Also an example for the application to caving mines is shown.

2 Comminution Model

In mineral processing, the kinetic milling model is widely applied to describe the breakage of particles. The parameters of this mathematical model are calibrated based on a set of experiments in which an initial size distribution is reduced in size. In that case, the matrix model is used to analyze the breakage of heterogeneous particles for any process that results in changes in the size distribution of the fragments (Broadbent and Callcot 1956). Assuming the breakage process as a succession of discrete events, two basic functions can be used to describe the progress of this process: the selection function and the breakage function. The selection function determines the proportion of particles that undergo breakage, while the remaining fragments are left unbroken. The probability that a particle of size y is broken to size x in the nth step of the breakage process is defined by breakage function, $B(x, y)$. The analysis of the breakage of brittle material confirmed that the rate that particles endure breakage is proportional to the mass reduction as a first order law (Austin and Concha 1994):

$$\frac{\mathrm{d}f_i(t)}{\mathrm{d}t} = -S_i f_i(t) \tag{1}$$

where f_i is the ore mass fraction in the ith size interval of the material being fragmented at time t and S_i is the proportionality constant known as "rate of breakage" or selection function with the unit of time^{-1}. The size of the class interval of material is defined based on the range of a sieve set. The sieve set should be selected in order to enable the classification of the new size distribution after

breakage. In the comminution model, the input size distribution of each breakage event is the output size of its previous step of breakage. Therefore, the resulting size distribution of the fragmented material in each breakage step can be represented by the accumulative fraction of the breakage product, B_{ij}, as (Austin and Concha 1994):

$$B_{ij} = \sum_{k=i}^{n} b_{kj} \tag{2}$$

where, b_{kj} is the fraction of material in the jth size interval which appears in the kth size interval after breakage: $b_{i,j} = B_{i,j} - B_{i+1,j}$. Both selection function—S_i in Eq. (1)—and breakage function—Eq. (2)—are used to predict the final size distribution in a fragmentation process. Indeed, the breakage probability of particles in any comminution device strongly depends on the strength properties, the particles size, and shape, and the homogeneity of material of the comminution system. The less spherical the particles, the greater the breakage will likely be. Furthermore, the larger particles have greater probability of being broken than the smaller particles. Thus, smaller particles require more events of breakage. Nevertheless, the coordination number (or number of particle to particle contact) also influences breakage, because the large particles have more contacts and then the load rests over more areas stabilizing this fragments (McDowell and Humphreys 2002).

2.1 Block Caving Comminution Model

The secondary fragmentation model presented in this paper is able to predict the particle size distribution applying the ore characteristics and operating conditions. The model structure is based on the population mass balance model, which has been widely accepted by researchers and is in common usage for many comminution systems (King 2001), including systems using the pressure as the main fragmentation mechanism (Torres and Casali 2009). The linear size-discretized model for breakage kinetics, in its general form, is defined as the ore mass fraction in the ith size interval, m_i, as follow (King 2001):

$$m_i = \int_0^{\infty} f_i(t)T(t)\mathrm{d}t \tag{3}$$

where $f_i(t)$ is the ore mass fraction in the ith size interval of the material being fragmented at time t and $T(t)$ is the residence time distribution. Equation (3) is known as the batch grinding kinetic equation and is expressed by the mass balance. In this equation, it is assumed that the breakage of material with greater size interval (jth) is proportional to the amount of material of size i in the mill as follows:

$$\frac{\mathrm{d}[m_{tot}f_i(t)]}{\mathrm{d}t} = -S_i m_{\mathrm{tot}} f_i(t) + \sum_{j=1}^{i-1} b_{ij} S_j m_{\mathrm{tot}} f_j(t) \tag{4}$$

where, m_{tot} is the total mass of material being fragmented, S_i is the selection function and denotes the fractional rate at which material is broken out of the ith size interval and b_{ij} is the breakage function and represents the fraction of the primary breakage product of material in the jth size interval of the feed material which appears in the ith size interval after fragmentation. Considering that during the extraction in a block cave, the cover load is expected to experience that constant vertical pressure (between 0 and 5 MPa) that is applied to the material; therefore, the axial mixing is not too severe. In this situation, it is appropriate to assume a plug flow. Since there is no mixing in plug flow, the output fragments have the same order they arrived into the system. Thus, the fragments entering the system at time, t, will exit the system at time $t + \tau$, where τ is the residence time. Considering the constant residence time for the system, Eq. (3) is re-written as follows:

$$m_i = f_i(\tau) \tag{5}$$

In Eq. (6), m_i is analytically defined for the N size classes and $t = \tau$ by substituting $f_i(t)$ from Eq. (4) by m_i and applying the batch grinding kinetic equation (Reid 1965). In this equation, m_{tot} is considered large enough to be assumed constant.

$$m_i = \sum_{j=1}^{i} A_{ij} e^{-S_j \tau} \tag{6}$$

where A_{ij} is expressed as follow in Eq. (7), S_j is the selection function at which material undergoes breakage to the jth size interval and τ is the residence time and denotes the time that material is under breakage process.

$$A_{ij} = \begin{cases} 0 & \text{if } i < j \\ f_{i0} - \sum_{k=1}^{i-1} A_{ik} & \text{if } i = j \\ \sum_{k=j}^{i-1} \frac{b_{ik} S_k}{S_i - S_j} A_{kj} & \text{if } i > j \end{cases} \tag{7}$$

where f_{i0} is the initial particle size distribution. Therefore, Eq. (6) allows predicting size distribution of a fragmentation process after b_{ij} (breakage function) and S_j (selection function) are determined. The functional expression of Austin and Luckie (1972) was applied to define the cumulative breakage form of the b_{ij} functions of the first event of breakage, B_{i1}:

$$B_{i1} = \alpha_1 \left(\frac{x_i}{x_2}\right)^{\alpha_2} + (1 - \alpha_1)\left(\frac{x_i}{x_2}\right)^{\alpha_3} \tag{8}$$

where α_1, α_2, and α_3 are model parameters ($0 < \alpha_1 < 1$; $\alpha_3 > \alpha_2$) representing the shape of the fragment size distribution and need to be fitted with the experimental data and x_i is a mesh size for a given size interval. There is no recirculation of fragments in caving operation. Then, if a proportion S_i is selected for breakage from f_i, the mass of fragments selected for breakage in size range i is represented by $S_i f_i$ and $(1 - S_i)f_i$ represents the fragment that remains unbroken. For the selection function, S_i, the functional expression presented in Eq. (9) was used (Herbst and Fuerstenau 1980), through S_i^E considered invariant for each size i:

$$S_i^E = S_1^E \exp\left\{ Z_1 \ln\left(\frac{d_i}{d_1}\right) + Z_2 \left[\ln\left(\frac{d_i}{d_1}\right)\right]^2 \right\} \tag{9}$$

where, Z_1, Z_2 and S_i^E are the model parameters. S_1^E represents the specific rate of breakage for particles of the maximum size fraction ($i = 1$), Z_1 and Z_2 represent the shape of the variation of the specific rate of breakage with particle size. These parameters need to be fitted with the experimental data. And d_i is the geometric mean of the ith size class, $d_i = \sqrt{x_i x_{i+1}}$. To obtain the selection function, S_i, a scale-up relationship (Herbst and Fuerstenau 1980) among the specific rate of breakage and the quotient between the power (P) and the total mass (m_{tot}) was used, as it is shown in Eq. (10).

$$S_i = S_i^E \left(\frac{P}{m_{\text{tot}}}\right) \tag{10}$$

As was mentioned above, in the case of Block Caving, m_{tot} was assumed constant, and it could be demonstrated that the relation of Power/m_{tot} could be equated to Pressure/constant, if power is considered by definition as force·velocity and pressure as force/area, and then with m_{tot} invariant, all constant values can be contained in S_i^E. Therefore, as S_i^E is invariant for each size, the scale-up relationship, Eq. (10), can be transformed to Eq. (11) as follows,

$$S_i = S_i^E(\sigma_{\text{V}}) \tag{11}$$

where σ_{V} is the vertical pressure in MPa owing to it is pressure controlled in experiment. In summary, the secondary fragmentation model of Block/Panel caving mines or, as called by the author, the Block Caving Comminution Model (BCCM) implements Eq. (6) to determine ore mass fraction at intervals previously defined. The model also requires the use of selection function, Eq. (11), for selecting fragments that will be broken and breakage function, Eq. (8), for determining the size distribution of these fragments. Hence, the model considers seven parameters α_1, α_2, α_3, τ, Z_1, Z_2 and S_i^E, that can be directly determined experimentally.

3 Laboratory Equipment, Material, and Experimental Conditions

3.1 Laboratory Setup

Confined flow experiments were conducted in order to study the secondary fragmentation. Experimental setup has been presented in (Castro et al. 2014). Equipment was selected that could deal with 60–70 kg of crushed ore per test. To avoid the concentration of stresses at corners, a cylindrical shape was selected for the model. A 1800 kN hydraulic press can apply high pressure to material confined in the cylinder, Fig. 1a. A steel cylinder with a

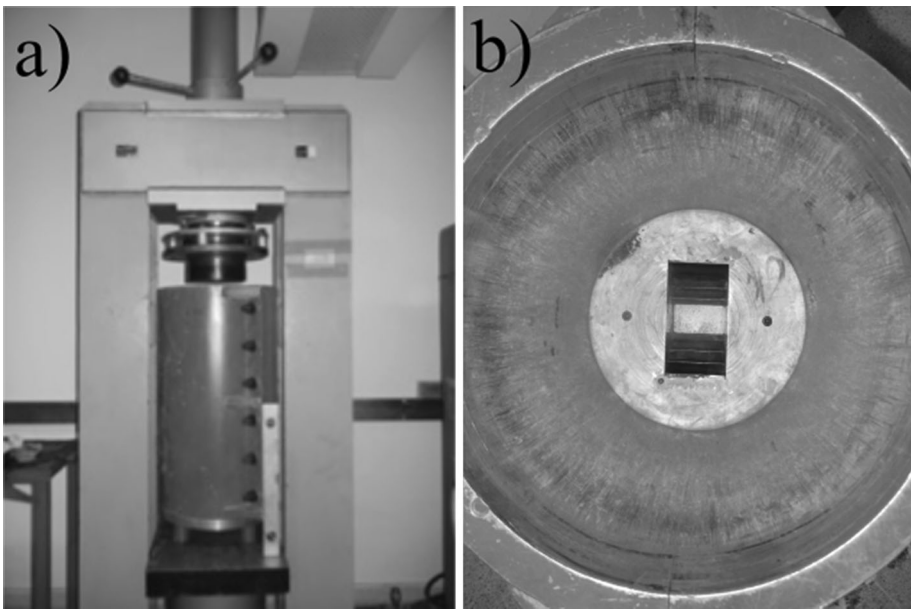

Fig. 1 **a** Cylindrical model in a press machine to apply different vertical pressures, σ_{v}. **b** Drawbell inside the physical model

340 mm inner diameter was selected to apply maximum pressure of 14 MPa (Fig. 1). The height of the cylinder was 700 mm, which was meant to hold the desired volume of ore and to suit the stroke length of the hydraulic press. In the base of the cylinder, there was a drawbell (1:75 scale) located in the center of the model to ensure that the flow zones would not intersect the model's walls (Fig. 1b). The outlet with a rectangular opening of 53 mm × 96 mm was set to allow the broken material to flow. The extraction system represents a Load Haul Dump (LHD) of 10.6 m^3 (14 yd^3).

3.2 Model Media

The material used in the experimental tests was crushed ore. Fragments' shape parameters, referring to methodology of Cho et al. (2006), consider a sphericity of 0.58 and a roundness of 0.25, in which sphericity represent the global form of the particle and reflects the similarity between the particle's length, height, and width, while roundness represents the scale of major surface features. Two different particle size distributions of sulfide ore were prepared and tested. The basic sample "a" with a wide distribution with d_{80} of 15.6 mm (Fig. 2) was scaled from the size distribution predicted for the Chuquicamata Underground Project, Chile (Codelco 2009). The other initial size distribution was constructed with the characteristic size (d_{80}) of 11.8 mm (Fig. 2, sample "b"). Additional material's characteristics used on experiments are summarized in Table 1, here considering both samples.

The model media consists of a sulfide ore corresponding to a biotite and amphibole granitoid, showing metallic mineralization of pyrite, chalcopyrite, and bornite. Also, samples showed an early stockwork (high-frequency network of small-scale veins; Brzovic and Villaescusa 2007) of quartz–feldespar veins with a potasic–feldspar alteration halo (Type A), thick quartz and gypsum veins as well as narrow quartz veins. Potasic and propilitic alteration can be seen in the rock samples and mafic minerals, respectively.

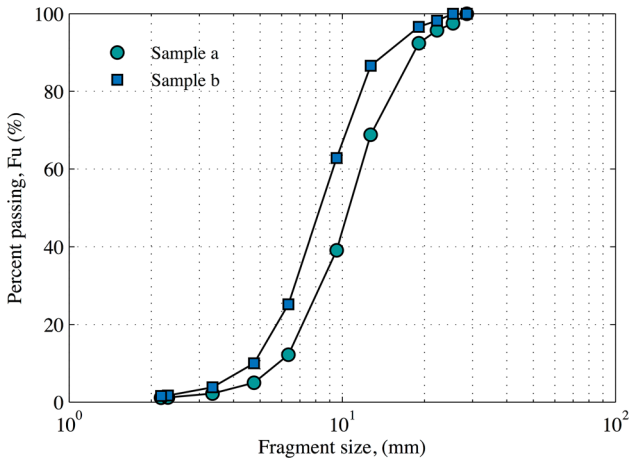

Fig. 2 Particle size distributions of samples: **a** $d_{80} = 15.6$ mm, **b** $d_{80} = 11.8$ mm

Table 1 Characteristics of the material tested

Parameter	Value	Unit
Coefficient of uniformity	2.0	Dimensionless
Density	2.62	t/m^3
Bulk density	1.90	t/m^3
Point load index	6.2	MPa
Internal friction angle	39	°

3.3 Experimental Methodology

A total of 18 experiments were run for each sample under drawn and undrawn conditions in the physical model described in Sect. 3.1. Here, material was drawn from one drawpoint of the drawbell located at bottom using a LHD system (lab scale). Material flowed continuously under isolated draw until 10% of total ore mass was extracted. This was due to the top of the material being reached by the movement zone. The size distributions were tested through sieves before and after testing. The experimental setups under which experiments were conducted are listed in Table 2. Vertical pressures were selected regarding different heights of the broken column to represent what is expected in caving operations. The Janssen formula (Nedderman 1992) was applied to calculate mean vertical pressures, $\overline{\sigma_v}$.

$$\overline{\sigma_v} = \frac{R_h \rho_b g}{\mathrm{Tan}(\varnothing_w) k} \left(1 - \exp^{\frac{-k\mathrm{Tan}(\varnothing_w) z}{R_h}}\right) \quad (12)$$

Table 2 Summary of the experimental setups

Test	Vertical pressure σ_V (MPa)	Initial size distribution		
		Sample	d_{80} (mm)	d_{50} (mm)
1	0	a	15.6	10.8
2	0.8		15.6	10.8
3	1.5		15.6	10.8
4	3		15.6	10.8
5	5		15.6	10.8
6	0	b	11.8	8.6
7	0.8		11.8	8.6
8	1.5		11.8	8.6
9	3		11.8	8.6
10	5		11.8	8.6

where R_h is the hydraulic radius (m), ρ_b is the bulk density (t/m^3), g is the gravitational constant (m/s^2), $\varnothing_w$ is the friction angle of the draw column boundary (rad), k is the ratio of horizontal to vertical stress, and z is the depth of the broken ore column (m).

4 Results

Initial and final fragmentations were measured in tests. The fragmentation after a confined flow test was determined by taking 25% of the total mass.

4.1 Reproducibility Evaluation

Duplicate tests were conducted in order to investigate the expected experimental errors. Figure 3a displays the result of tests 3 and 8 ($\sigma_v = 1.5$ MPa) and their duplicate tests (3.1 and 8.1), while Fig. 3b displays the result of tests 4 and 9 ($\sigma_v = 3$ MPa) and their duplicate tests (4.1 and 9.1).

Tests under vertical pressures of 1.5 MPa show a correlation coefficient of 98.6 and 99.8% (Fig. 3a, tests 3 and 8, respectively). In addition, tests under 3 MPa show a correlation coefficient of 99.9 and 99.6% (Fig. 3b, tests 4 and 9, respectively).

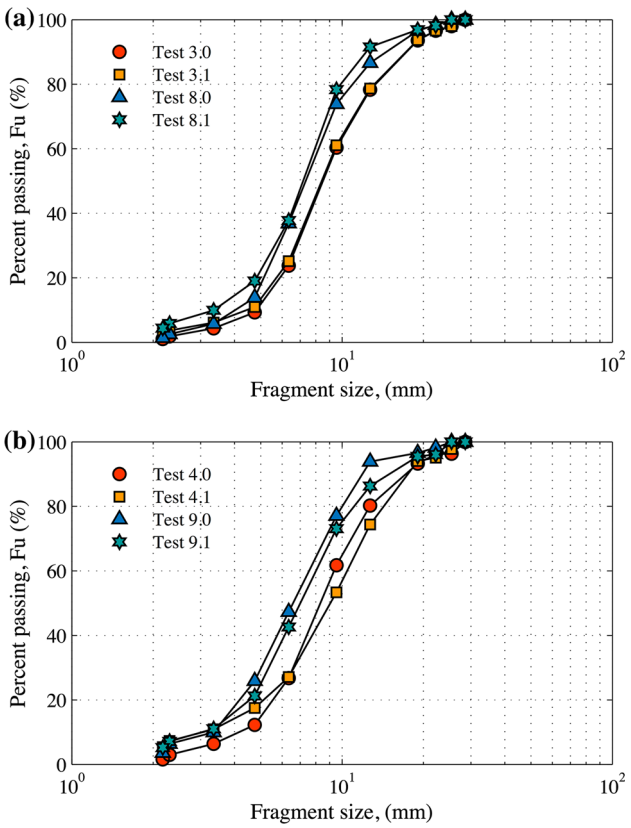

Fig. 3 Experimental tests reproducibility

4.2 Extraction Effect

Experiments at 3 MPa were conducted to quantify the influence of compaction and draw on secondary fragmentation. The experiments in which draw was considered involved the extraction of 10% of the total mass. Figure 4 shows results for both conditions. It was observed that breakage due to draw is relevant and involved a reduction on size due to abrasion. In Table 3 the reduction according to size is presented, and as noted the larger the fragments, the larger was the amount of breakage due to flow. Smaller fragments were reduced more by compaction than they were by flow.

4.3 Fragmentation Results

Compression and abrasion were the main breakage mechanisms in experiments. Both are differentiated in Sect. 4.2. Particle breakage was observed in range of pressures applied (between 0.8 and 5 MPa) although these values are minor compared to ore strength (uniaxial compressive strength and uniaxial tensile strength around to 142 MPa and 7.8 MPa, respectively, both determined through the point load index measured; Franklin 1985). A reasonable explanation for this has to do with point loads due to stress distribution of particles, where a high concentration of force takes place through a small contact zone between fragments. It is consistent with studies of aggregate particle crushing where the probability of particle survival as a function of stress applied for a specific fragment size (e.g., 20 mm), $P_s(\sigma)$, or the probability of breakage in this case, $1 - P_s(\sigma)$, it is between 41 and 60% from 0.8 to 5 MPa, respectively (McDowell and Bolton 1998; Nakata et al. 1999; McDowell and Humphreys 2002).

After conducting extraction, fragmentation curves were obtained. Example of these curves for different vertical

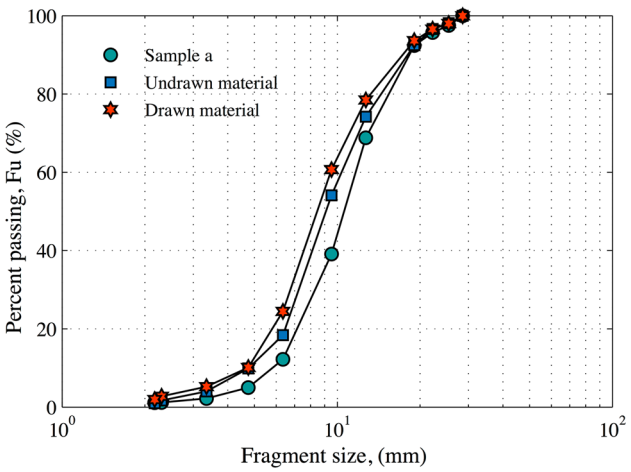

Fig. 4 Fragmentation due to draw, vertical pressure of 3 MPa

Table 3 Size breakage between undrawn and drawn condition

Sizes	Initial sample a (mm)	Compaction (mm)	% Breakage	Compaction and draw (mm)	% Breakage
d_{80}	1.17	1.09	6.8	1.00	14
d_{50}	0.81	0.69	14.8	0.66	18
d_{10}	0.45	0.36	20	0.35	22.2

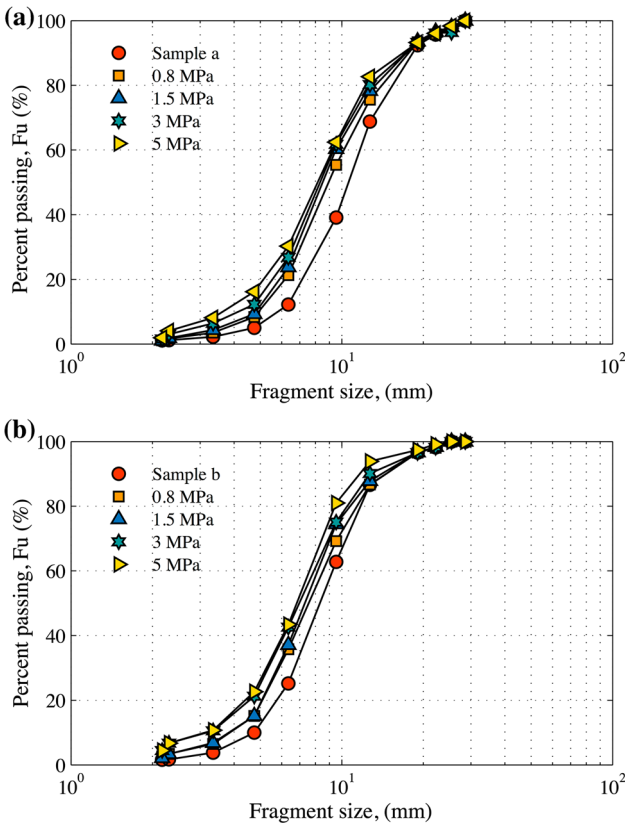

Fig. 5 **a** Fragmentation results of sample "*a*" ($d_{80} = 15.6$ mm). **b** Fragmentation results of sample "*b*" ($d_{80} = 11.8$ mm)

pressures are shown in Fig. 5, where samples "a" defined an initial $d_{50} = 10.8$ mm and "b" an initial $d_{50} = 8.6$ mm. The results show that the higher the vertical pressure the higher the breakage. In terms of particle size, the coarser material fragments show a greater percentage of reduction in fragmentation (Table 4).

The characteristic passing size (d_{10}, d_{50} and d_{80}) of the two samples are presented in Table 4 as a function of vertical pressure. The results indicate that the larger degree of breakage occurs for the smaller passing size (d_{10}) reaching over 30% for 3 MPa. On the other hand, the larger characteristic size (d_{80}) shows a smaller degree of breakage (%). The change of the shape of the fragmentation curves were also quantified in terms of their coefficient of

Table 4 Characteristic fragment size as a function of vertical pressure for samples a and b

Pressure (MPa)	d_{10} (mm)	d_{50} (mm)	d_{80} (mm)	$C_u = d_{60}/d_{10}$
Sample a				
Initial	5.95	10.80	15.63	2
0.8	5.02	9.12	14.18	2
1.5	4.72	8.74	13.27	2
3	4.03	8.59	12.66	2.3
5	3.72	8.41	12.28	2.5
Sample b				
Initial	4.75	8.61	11.83	2
0.8	4.01	7.80	11.46	2.2
1.5	3.96	7.56	10.79	2.1
3	3.21	7.12	10.53	2.5
5	3.16	6.96	9.45	2.5

uniformity ($C_u = d_{60}/d_{10}$). The results indicate the C_u increases with vertical pressure; therefore, more fine material is produced.

4.4 Modeling

Parameters described in Sect. 2.1 were fitted through fragmentation result. These values were common in both samples because they were the same material and they were under the same fragmentation process. The fitting was performed by minimizing square error. The selection function fitted to the experiments is plotted in Fig. 6a as well as the breakage function in Fig. 6b. The selection function is modeled by the polynomial previously described in Eq. (9). Here, it can be observed that the larger fragments have a higher rate of breakage, which means larger fragments have a greater probability of breakage until they reach a certain size, after which this probability decreases. The breakage reduction of larger sizes could be explained due to their bigger number of contacts (McDowell and Humphreys 2002).

The model's parameters obtained from experiments are displayed in Table 5. Parameter τ represents the residence time in a comminution machine, so it could not have been a necessary constant, these are discussed in Sect. 5.2.

Values shown in Table 5 are the fitting parameters determined through Eq. (6) and experimental data. The selection function Eq. (9) is a second-grade polynomial shown in Fig. 6a parameterized with S_i^E, Z_1, Z_2. Here, S_i^E represents the amount of larger particles that will be fragmented. And this parameter is the starting point for other minor sizes, $i + 1$. If S_i^E is large, then it also increases the amount of particles undergoing breakage from sizes $i + 1$, while Z_1 and Z_2 are second-grade polynomial constants that defined the polynomial's curve.

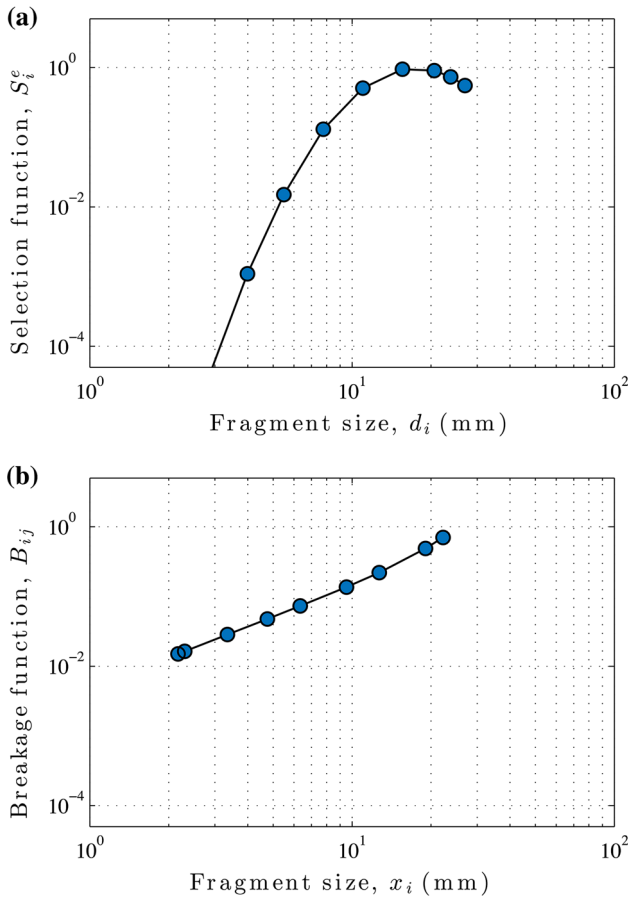

Fig. 6 **a** Experimental selection function and **b** experimental breakage function

Table 5 Fitted parameters of the comminution model

S_i^E	Z_1	Z_2	α_1	α_2	α_3	τ
0.551	−2.668	−3.082	0.545	1.46	4.375	0.239

The resulting size distribution or the proportion of particles that will be fragmented (defined previously by the selection function) is determined through the breakage function Eq. (8), B_{i1}, shown in Fig. 6b for the first event of breakage. The breakage function depends on α_1, α_2 and α_3, when α_1 increases it also increases the fragmentation and vice versa. On the contrary, when α_2 and α_3 increase, this implies minor fragmentation. How the proportion of size particles are selected for breakage depends on the selection function. The major or minor fragmentation described for breakage parameters is relative to the size distribution. This majority fragmentation refers to the majority proportion of minor sizes.

In order to evaluate the Block Caving Comminution Model described above, size distribution curves (accumulated material, F_u) obtained in tests are plotted. Figure 7 displays size distributions of the model as well as experimental results. It is observed that the model could be used to fit the observed fragmentation including the vertical pressures effect for different ranges. Figures show good fitting in both higher and lower sizes of the curves.

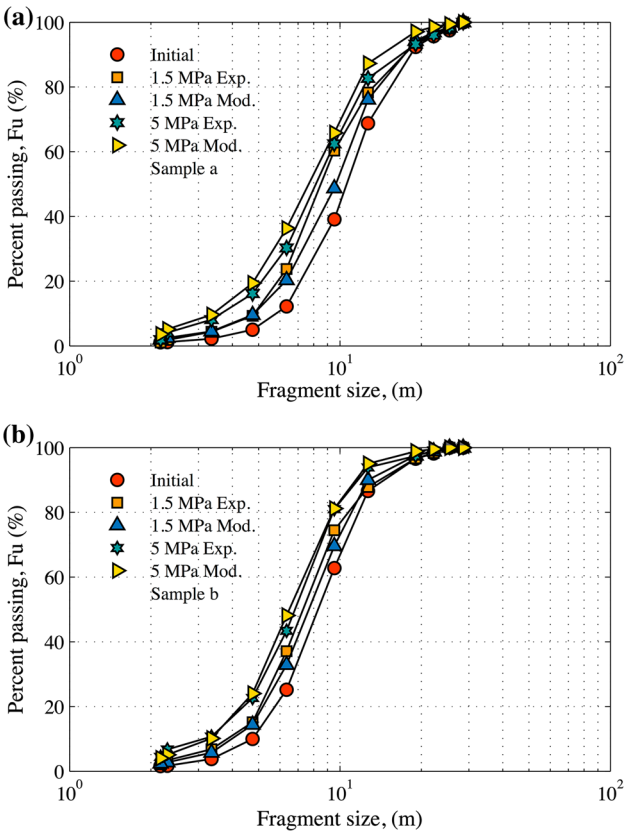

Fig. 7 **a** Some experimental results of sample "*a*" compared with BCCM. **b** Some experimental results of sample "*b*" compared with BCCM

The goodness of fit of the model was determined by applying the correlation coefficient, R^2, as well as the mean squares error (MSE),

$$\mathrm{MSE} = \frac{1}{N}\sum_{i=1}^{N}\left(y_{i,\mathrm{exp}} - y_{i,\mathrm{mod}}\right)^2 \tag{13}$$

where, N is the total number of sizes fraction, $y_{i,\mathrm{exp}}$ is the cumulative size fractions for size i measured and $y_{i,\mathrm{mod}}$ is the cumulative size fractions for size i modeled. The correlation coefficients and the MSE values presented in Table 6 show that the Block Caving Comminution Model could effectively represent the modeling size distribution results obtained by a breakage process. In this instance, it represents the secondary fragmentation under confined flow.

Table 6 Model goodness of fit

Test	Sample	Vertical pressure (MPa)	Correlation coefficient R^2 (%)	MSE (%^{2})
1	a	0.8	99.75	12.42
2		1.5	99.69	12.65
3		3	99.94	2.31
4		5	99.89	11.34
5	b	0.8	99.90	5.99
6		1.5	99.90	4.13
7		3	99.97	4.11
8		5	99.95	2.16

5 Mine Application

5.1 Block Caving Comminution Model Based on Field Data

The El Teniente mine was considered to evaluate the Comminution model (sectors: Esmeralda and Reno). The fragmentation of these sectors was compared with the Block Caving Comminution Model. The model's parameters obtained in Chapter 4 were used, BCCM (exp).

Fragmentation of Esmeralda sector measured during three recent years is illustrated in Fig. 8 (Codelco 2015). The size distribution curve of 2013 represents fragmentation from 0 to 20 m of an extraction column and it was considered as the initial curve for BCCM predictions. Also in Fig. 8, BCCM's outcomes are shown.

The mean estimated accuracy of the percent passing, F_u, is 1.54% for BCCM (exp). It can be noticed that BCCM's parameters have not been scaled up; moreover, the experimental setup represents a small footprint (one drawpoint) compared with mine scale where ore is drawn through

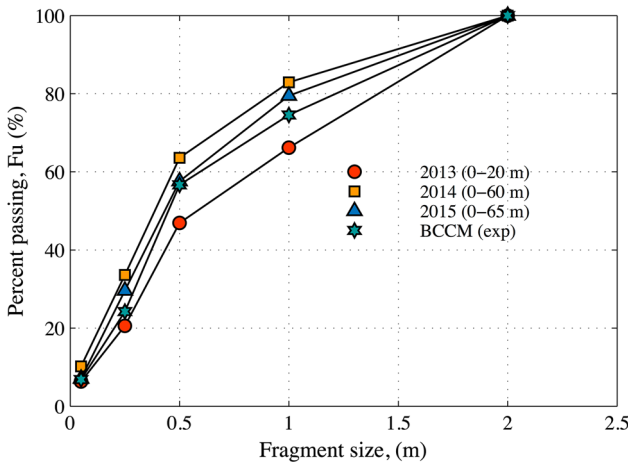

Fig. 8 Fragmentation curves of Esmeralda, El Teniente mine and the BCCM

various drawpoints. However, an adequate prediction is observed. Probably, this fact is because the scale factor was considered in the selection function (Austin and Concha 1994) through power/m_{tot}, which in the BCCM has been related to vertical pressure, σ_v, and this parameter is directly applied to the physical model at mine ranges.

5.2 Height Consideration

Secondary fragmentation is highly influenced by ore transport in the ore caved column. When fragments come from higher up in the column, they have to stay in the column for a longer time. In the Block Caving Comminution Model, this is taken into account by applying the fragmentation recursively as the draw progresses. But vertical pressure is also a key parameter in the model presented, so for different heights the model considers different residence time, τ, and different vertical pressures, σ_v.

As shown in Fig. 9 in the BCCM, the broken column height is discretized in smaller heights (Z_i), where each is associated with a particular residence time and vertical pressure. This could be observed, for example, in the first zone, Z_0, where secondary fragmentation has not taken effect at the beginning of caving process. At this height, vertical pressure is insignificant because the caved column is currently growing, and there are short distances between ore fragments and drawpoints, so fragments have a low chance of being affected by breakage events. During the progress of ore extraction, the caved column increases its height (and draw area as well) implying higher vertical pressure, which can be estimated through Janssen's approach presented in Sect. 3.3. Fragmentation will decrease in the following zones by progressing ore extraction as various studies reveal (Eadie 2003; Calder et al. 2000; Srikant and Rachmad 2004; Hurtado and Pereira 2009; Montecino 2011; Viera and Diez 2014).

In order to incorporate predictions for different extraction periods, data from Reno (El Teniente mine) are used where fragmentation information is available as a function of column height in (Hurtado and Pereira 2009). Figure 10 shows particle size distributions of the Hanging wall "Hw" sector of Reno (Fig. 10).

Here, these fragmentation curves are considered for 0–50 m (as initial curve), 150–100, 0–200, 0–300 and 0–400 m of draw columns. The Block Caving Comminution Model was run for the initial curve with parameters defined in Table 5 with the exception of τ which is fixed for each height of draw, so then, τ is linearly related with the height of draw as shown in Fig. 11.

Consequently, the τ parameter relationship was adjusted with Reno's data. It is expressed through the draw column height and the rate of draw, as follows:

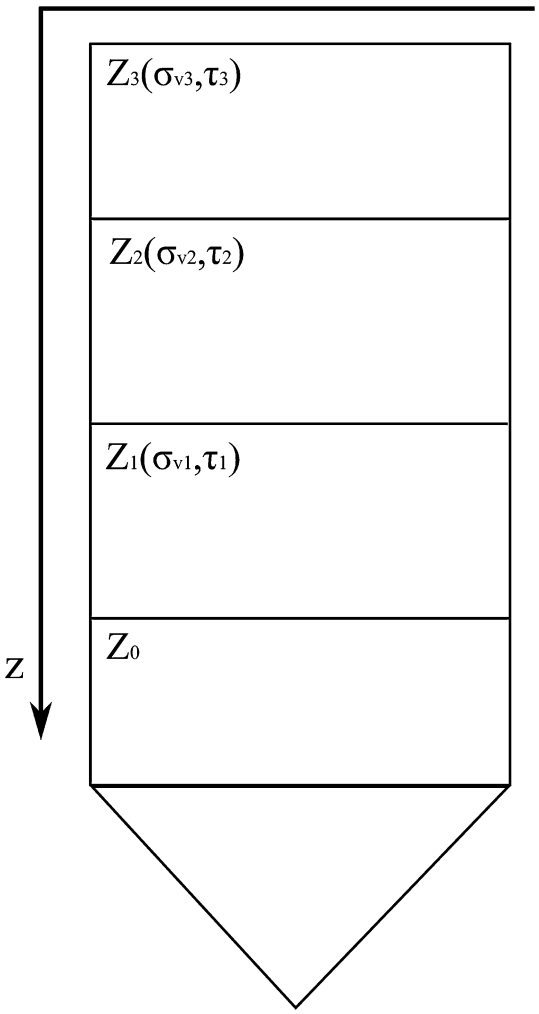

Fig. 9 Schematic view of areas for fragmentation prediction at various heights of draw column

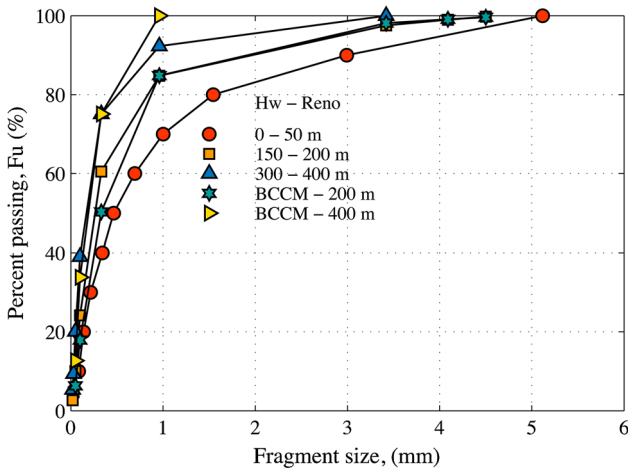

Fig. 10 Fragmentation back-analysis from Reno (Hurtado and Pereira 2009) and the BCCM estimations

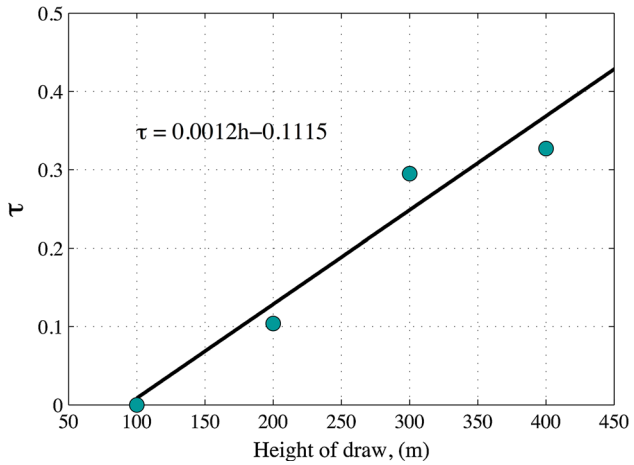

Fig. 11 Residence time parameter, τ, as function of the height of draw

$$\tau = 0.239\left(\frac{\rho_b}{R_d}\frac{H}{C_1}\right) + C_2 \tag{14}$$

where ρ_b is the bulk density of the broken ore (t/m^3), H is the height of the draw column (m), R_d is the rate of draw or extraction rate (t/m^2/d) and C_1 and C_2 are dimensionless constants. Here constant parameters C_1 and C_2 are 3095 and -0.112, respectively; however, these values could change for different mines. The meaning that authors give to these constants is for C_1, discretizes the height of the draw column and reduces the magnitude of height to τ magnitude, while C_2 should be the value of τ when secondary reduction hasn't happened yet. The residence time parameter τ in Eq. (14) and the mean vertical pressure estimated through Eq. (12), both of which are considered in the BCCM, can be used for secondary fragmentation predictions at different draw column heights or at different extraction periods.

6 Conclusions

Reaching an acceptable prediction of the final size distribution in drawpoints is not simple due to the number of parameters and processes involved in ore fragmentation in Block Caving. This paper seeks to postulate a predictive model for secondary fragmentation through the implementation of the Block Caving Comminution Model. It is based on the mineral comminution of the fragmentation that occurs in grinding machines as applied to caving mines. The vertical pressure is considered and model's parameters are calibrated through a confined flow model which gives fragmentation results according to vertical pressure applied.

The main advantages of this model are its capacity to adopt any shape of the size distribution curves, and to

incorporate the period of extraction through both the vertical pressure and the residence time parameter. A further advantage is that the fragmentation results obtained in the laboratory can be easily scaled by the vertical pressure of broken column.

The experimental methodology allows the secondary fragmentation to be estimated. However, in this work, a specific type of material was used for different material characteristics; therefore, the Block Caving Comminution Model's parameters should be calibrated in the confined model for the material desired. However, closed parameter results would be expected if the materials considered were primary ore.

Acknowledgements This paper describes a component of the work carried out within the project "Gravity flow technologies and fundamentals" run by the University of Chile Advanced Mining Technology Center and funded by the Chilean government through the CONICYT Project FB0809. The authors would like to thank Dr. Andrés Brzovic for his support in the presented article sharing this valuable mine experience from El Teniente mine.

Appendix: Comminution Model Example

In this example, the model's parameters presented in Table 5 are used, considering a vertical pressure of 3 MPa and the initial size distribution curve with five size intervals, $i = \{1,2, \ldots, 5\}$, shown in Table 7.

The residence time parameter, τ, can be determined based on Eq. (14) depending on the draw column geometry. For example, it can be determined for a draw column of 200 m height, a bulk density of 1.9 t/m^3 and a rate of draw of 0.45 t/m^2/d,

$$\tau = \left(\frac{1.9}{0.45}\frac{H}{3095}\right) - 0.112 = 0.16.$$

Then, Eq. (6) is used to estimate the ore mass fraction in the size intervals of Table 7,

$$p_i = \sum_{j=1}^{i} A_{ij} e^{-S_j 0.16}$$

where

Table 7 Initial size distribution curve-example

Upper size (m)	Geometric mean size (mm)	F_u (%)	f_{i0} (%)
2	1.41	100	15
1	0.71	85	25
0.5	0.35	60	40
0.25	0.11	20	20
0.05	0	0	0

$$A_{ij} = \begin{cases} 0 & \text{if } i < j \\ f_{i0} - \sum_{k=1}^{i-1} A_{ik} & \text{if } i = j \\ \sum_{k=j}^{i-1} \frac{b_{ik} S_k}{S_{i-} S_j} A_{kj} & \text{if } i > j. \end{cases}$$

The selection function is described by Eqs. (9) and (11) considering the vertical pressure, σ_v,

$$S_i^E = 0.551 \exp\left\{-2.668 \ln\left(\frac{d_i}{1.41}\right) - 3.082\left[\ln\left(\frac{d_i}{1.41}\right)\right]^2\right\} 3$$

$$S_i^E = \begin{matrix} 1.653 \\ 2.390 \\ 0.179 \\ 0.000 \\ 0.000 \end{matrix}$$

Besides, the breakage function of the first breakage event is described by Eq. (8).

$$B_{i1} = 0.545\left(\frac{x_i}{x_2}\right)^{1.46} + (1 - 0.545)\left(\frac{x_i}{x_2}\right)^{4.375}.$$

Then, it can be calculated b_{ij} on intervals after $i = 1$ (i.e., $i = \{2, 3, 4, 5\}$). The distribution for the size intervals after a breakage process has the same behavior,

$$B_{i1} = \begin{matrix} 1 \\ 1 \\ 0.220 \\ 0.073 \\ 0.007 \end{matrix} \quad b_{ij} = \begin{matrix} 0 & 0 & 0 & 0 \\ 0.780 & 0 & 0 & 0 \\ 0.147 & 0.780 & 0 & 0 \\ 0.066 & 0.147 & 0.780 & 0 \\ 0.007 & 0.073 & 0.220 & 1 \end{matrix}$$

When the distribution of fragments that are selected to be broken is known, A_{ij} is calculated as:

$$A_{ij} = \begin{matrix} f_{i0} - \sum_{k=1}^{0} A_{1k} & 0 & 0 & 0 & 0 \\ \sum_{k=1}^{1} \frac{b_{2k} S_k}{S_{2-} S_1} A_{k1} & f_{2,0} - \sum_{k=1}^{1} A_{2k} & 0 & 0 & 0 \\ \sum_{k=1}^{2} \frac{b_{3k} S_k}{S_{3-} S_1} A_{k1} & \sum_{k=2}^{2} \frac{b_{3k} S_k}{S_{3-} S_2} A_{k2} & f_{3,0} - \sum_{k=1}^{2} A_{3k} & 0 & 0 \\ \sum_{k=1}^{3} \frac{b_{4k} S_k}{S_{4-} S_1} A_{k1} & \sum_{k=2}^{3} \frac{b_{4k} S_k}{S_{4-} S_2} A_{k2} & \sum_{k=3}^{3} \frac{b_4 S_k}{S_{4-} S_3} A_{k3} & f_{4,0} - \sum_{k=1}^{3} A_{4k} & 0 \\ \sum_{k=1}^{4} \frac{b_{5k} S_k}{S_{5-} S_1} A_{k1} & \sum_{k=2}^{4} \frac{b_{5k} S_k}{S_{5-} S_2} A_{k2} & \sum_{k=3}^{4} \frac{b_{5k} S_k}{S_{5-} S_3} A_{k3} & \sum_{k=4}^{4} \frac{b_{5k} S_k}{S_{5-} S_4} A_{k4} & f_{5,0} - \sum_{k=1}^{4} A_{5k}. \end{matrix}$$

Replacing f_{i0}, b_{ij} and S_i,

$$A_{ij} = \begin{matrix} 0.150 \\ 0.263 & -0.013 \\ -0.357 & 0.011 & 0.746 \\ -0.036 & 0.001 & -0.582 & 0.816 \\ -0.020 & 0.001 & -0.110 & -0.637 & 0.766 \end{matrix}$$

Finally, replacing f_{i0}, S_i and in Eq. (5),

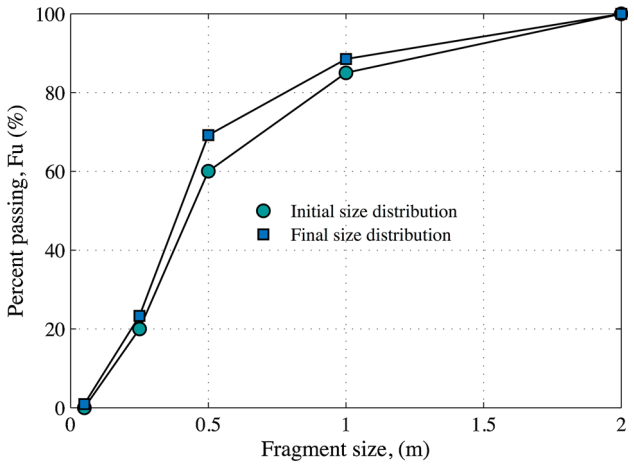

Fig. 12 Block Caving Comminution Model example

$$m_i = \begin{matrix} 11.51 \\ 19.30 \\ 45.85 \\ 22.43 \\ 0.76 \end{matrix}$$

Figure 12 shows the fragmentation curve of the example through the cumulative size distribution.

References

Austin L, Concha F (1994) Discrete mill kinematic: population mass balance of sizes. In: Austin L, Concha F (eds) Design and simulation of mill and classification circuits. CYTED, Concepcion, pp 65–82 (**in Spanish**)

Austin L, Luckie PT (1972) Estimation of non-normalized breakage distribution parameters from batch grinding. Powder Technol 5(5):267–271

Bridgwater J, Utsumi R, Zhang Z, Tuladhar T (2003) Particle attrition due to shearing—the effects of stress, strain and particle shape. Chem Eng Sci 58(20):4649–4665

Broadbent SR, Callcot TG (1956) A matrix analysis of processes involving particle assemblies. Philos Trans R Soc Lond Math Phys Sci 249(960):99–123

Brown ET (2004) Fragmentation assessment. In: Brown E (ed) Block caving geomechanics, 2nd edn. JKMRC, Queensland, pp 184–227

Brzovic A, Villaescusa E (2007) Rock mass characterization and assessment of block-forming geological discontinuities during caving of primary copper ore at the El Teniente mine, Chile. Int J Rock Mech Min Sci 44(4):565–583

Calder K, Townsend P, Russell F (2000) The Palabora underground mine project. In: Proceedings MassMin 2000. Brisbane, pp 219–225

Castro R, Fuenzalida MA, Lund F (2014) Experimental study of gravity flow under confined conditions. Int J Rock Mech Min Sci 67:164–169

Chitombo G (2010) Cave mining—16 years after Laubscher's 1994 paper "cave mining—state of the art". In: Potvin Y (ed) Proceedings of the 2nd international symposium on block and sublevel caving. Perth, pp 45–61

Cho G, Dodds D, Santamarina JC (2006) Particle shape effects on packing density, stiffness and strength: natural and crushed sands. J Geotech Geoenviron Eng 132(5):591–602

Codelco (2009) Prefeasibility study of Chuquicamata underground mine project. Technical report, Main Decisions, MSC-ICO-SKMMIN-0000-GEN-INF-100, Vicepresindecia Corporativa de Proyectos **(in Spanish)**

Codelco (2015) Fragmentation back-analysis: sector Esmeralda. Technical report, Division El Teniente, Coldelco **(in Spanish)**

Eadie B (2003) A framework for modelling fragmentation in block caving. PhD thesis, The University of Queensland

Esterhuizen GS (2005) A program to predict block cave fragmentation. Technical reference and Useŕs Guide Version 3.05

Flores G (2014) Future challenges and why cave mining must change. In: Castro R (ed) 3rd International symposium on block and sublevel caving. Santiago, pp 23–52

Franklin JA (1985) Suggested method for determining point load strength. Int J Rock Mech Min Sci Geomech Abstr 22(2):51–60

Hardin BO (1985) Crushing of soil particles. J Geotech Eng 111(10):1177–1192

Herbst JA, Fuerstenau DW (1980) Scale-up procedure for continuous grinding mill design using population balance models. Int J Miner Process 7(1):1–31

Hurtado JP, Pereira J (2009) Fragmentation back-analysis: Sector Reservas Norte. Technical report, Division El Teniente, Coldelco

King RP (2001) Modelling and simulation of mineral processing systems. Butterworth

Laubscher DH (1994) Cave mining-the state of the art. J South Afr Inst Min Metall 94(10):279–293

McDowell GR, Bolton MD (1998) On the micromechanics of crushable aggregates. Geotechnique 48(5):667–679

McDowell GR, Humphreys A (2002) Yielding of granular materials. Granular Matter 4(1):1–8

Merino L (1986) Predicting the size distribution of ore fragments in block caving mines. Master thesis, Imperial College, England

Montecino N (2011) Mixing model of secondary fragmentation in block/panel caving mining. Master thesis, University of Chile, Chile **(in Spanish)**

Nakata Y, Hyde A, Murata H (1999) A probabilistic approach to sand particle crushing in the triaxial test. Geotechnique 49(5):567–583

National Materials Advisory Broad (1981) Comminution and energy consumption. Report No 364, U.S. Dept. of Energy, U.S. Bureau of mines, National Science Foundations

Nedderman RM (1992) The Method of differential slices. In: Nedderman R (ed) Statics and Kinematics of Granular Material. Cambridge University Press, New York, pp 84–126

Ngidi S, Pretorius D (2010) Impact of poor fragmentation on cave management. In: Potvin Y (ed) Proceedings of the 2nd international symposium on block and sublevel caving. Perth, pp 593–601

Pierce ME (2009) A model for gravity flow of fragmented rock in block caving mines. PhD thesis, The University of Queensland

Pierce ME, Waetherley DK, Kojovic TA (2010) A hybrid methodology for secondary fragmentation prediction in cave mines. In: Potvin Y (ed) Proceedings of the 2nd international symposium on block and sublevel caving. Perth, pp 567–582

Reid KJ (1965) A solution to the batch grinding equation. Chem Eng Sci 20(11):953–963

Srikant A, Rachmad L (2004) Visual estimation of fragment size distributions in the DOZ block cave. In: Proceeding of the 4th international conference and exhibition on mass mining 2004. Santiago, pp 286–290

Torres M, Casali A (2009) A novel approach for the modelling of high-pressure grinding rolls. Miner Eng 22(13):1137–1146

Viera E, Diez E (2014) Analysis of hang up frequency in Bloque 1-2, Esmeralda Sur Mine. In: Castro R (ed) 3rd International symposium on block and sublevel caving. Santiago, pp 138–145